DOI: 10.14814/phy2.14449

ORIGINAL RESEARCH

Physiological Reports

Calcium-induced calcium release in proximity to hair cell BK channels revealed by PKA activation

Jun-ping Bai[1] | **Na Xue**[2] | **Omolara Lawal**[1] | **Anda Nyati**[3] | **Joseph Santos-Sacchi**[4,5,6] | **Dhasakumar Navaratnam**[1,4,6]

[1]Department of Neurology, Yale School of Medicine, New Haven, CT, USA

[2]Department of Otolaryngology-Head and Neck Surgery, Shanghai Ninth People's Hospital, Shanghai Jiaotong University School of Medicine, Shanghai, China

[3]Undergraduate Program, Johns Hopkins University, Baltimore, MD, USA

[4]Department of Surgery, Yale School of Medicine, New Haven, CT, USA

[5]Department of Cell and Molecular Physiology, Yale School of Medicine, New Haven, CT, USA

[6]Department of Neuroscience, Yale School of Medicine, New Haven, CT, USA

Correspondence
Dhasakumar Navaratnam, Departments of Neurology, Neuroscience and Surgery, Yale School of Medicine, New Haven, CT, USA.
Email: Dhasakumar.Navaratnam@Yale.Edu

Funding information
This work was funded by the NIH/ NIDCD R01 R01DC007894 to DSN.

Abstract

Large-conductance calcium-activated potassium (BK) channels play a critical role in electrical resonance, a mechanism of frequency selectivity in chicken hair cells. We determine that BK currents are dependent on inward flow of Ca^{2+}, and intracellular buffering of Ca^{2+}. Entry of Ca^{2+} is further amplified locally by calcium-induced Ca^{2+} release (CICR) in close proximity to plasma membrane BK channels. Ca^{2+} imaging reveals peripheral clusters of high concentrations of Ca^{2+} that are suprathreshold to that needed to activate BK channels. Protein kinase A (PKA) activation increases the size of BK currents likely by recruiting more BK channels due to spatial spread of high Ca^{2+} concentrations in turn from increasing CICR. STORM imaging confirms the presence of nanodomains with ryanodine and IP3 receptors in close proximity to the Slo subunit of BK channels. Together, these data require a rethinking of how electrical resonance is brought about and suggest effects of CICR in synaptic release. Both genders were included in this study.

KEYWORDS

BK channels, CICR, Hair Cell, STORM imaging

1 | INTRODUCTION

Large-conductance potassium channels (BK) play an essential role in hair cell physiology. In mammalian inner hair cells, these channels are the largest contributor to its outward current (Marcotti, Johnson, Holley, & Kros, 2003; Marcotti, Johnson, & Kros, 2004). In mammalian outer hair cells, these channels lie in proximity to nicotinic receptors and serve to set the resting membrane potential (Fuchs & Lauer, 2019; Rohmann, Wersinger, Braude, Pyott, & Fuchs, 2015). In non-mammalian vertebrates, BK channels play an essential role in electrical resonance, a mechanism of frequency selectivity (Art, Wu, & Fettiplace, 1995; Duncan & Fuchs, 2003; Fettiplace & Fuchs, 1999; Fuchs & Evans, 1990).

In the best-studied example of turtles, electrical resonance is brought about by an interplay of an inward current through voltage-gated Ca^{2+} channels, and an outward current from large-conductance Ca^{2+}-activated potassium

Jun-ping Bai and Na Xue authors contributed equally to this work.

(BK) channels (Fettiplace & Fuchs, 1999). These two channels lie in close proximity to one another and bring about oscillation in membrane potential (Fettiplace & Fuchs, 1999; Roberts, Jacobs, & Hudspeth, 1990). The frequency of membrane potential oscillation varies as a function of tonotopicity (Crawford & Fettiplace, 1981). In the turtle, this change in frequency is in turn brought about by variation in the number of channels and, more importantly, a change in the kinetics of the BK channel (Fettiplace & Fuchs, 1999). These data have been mainly corroborated in the chick auditory epithelium (Duncan & Fuchs, 2003; Fettiplace & Fuchs, 1999).

How might the changes in BK channel kinetics be brought about? The early promise of varying primary structure of the alpha subunit of the BK channel from changing alternative splicing along the tonotopic axis failed to explain the variation in channel kinetics (Jones, Gray-Keller, Art, & Fettiplace, 1999; Miranda-Rottmann, Kozlov, & Hudspeth, 2010; Ramanathan, Michael, Jiang, Hiel, & Fuchs, 1999). Changes in association with auxiliary proteins and changes in kinase activity along the tonotopic axis are two other mechanisms that could account for the alterations in the kinetic properties of the BK channel. Prior data have shown expression of KCNMB1 and KCNMB4 in the low-frequency end of the basilar papilla (Bai, Surguchev, & Navaratnam, 2011; Ramanathan, Michael, & Fuchs, 2000), and, indeed, we demonstrated changes in CDK5 expression along the tonotopic axis (Bai, Surguchev, Joshi, Gross, & Navaratnam, 2012b). Furthermore, higher PKA expression at the low-frequency end of the tonotopic axis is suggested by global gene expression analysis along the tonotopic axis (Frucht, Uduman, Kleinstein, Santos-Sacchi, & Navaratnam, 2011).

In this paper, we sought to determine how PKA activity affects BK channel kinetics in tall hair cells that receive principally afferent innervations. Our unexpected finding was that PKA recruited BK channels by inducing calcium-induced calcium release (CICR). Using super-resolution microscopy, we determine expression of clusters of both IP3 and ryanodine receptors along the plasma membrane of these cells in proximity to Slo, the alpha subunit of BK channels. These data have implications for the speed and amplification of feedback loops governing electrical tuning, and for synaptic vesicle release.

2 | METHODS

All the studies were done in accordance with the National Institutes of Health Guide for the Care and Use of Laboratory Animals, and the protocols were applied in compliance with the Yale University institutional review board guidelines.

2.1 | Electrophysiological recording

Whole-cell patch-clamp recordings were made of tall hair cells from freshly isolated basilar papilla from E21 chicks of either sex, when hearing is mature (Fuchs & Sokolowski, 1990; Jones & Jones, 1995; Saunders, Coles, & Gates, 1973). Hair cells were exposed as previously described (Ricci et al., 2013). Recordings were obtained in the whole-cell configuration. Hair bundle heights were measured as a reference to its tonotopic location (Tilney, Tilney, Saunders, & DeRosier, 1986). Cells were recorded in the presence of blockers of KCNQ (100 μM linopirdine) and SK channels (300 nM apamin) to isolate BK currents. The extracellular solution was as follows (in mM): 144 NaCl, 0.9 $MgCl_2$, 1.3 $CaCl_2$, 1.0 KCl, 0.7 NaH_2PO4, 10 HEPES, and 5 glucose, pH 7.4 and 300 mOsm. The composition of the pipette solution was (in mM): 120 K-gluconate, 20 KCl, 5 EGTA, 5 HEPES, 2.5 Na2ATP, 3.5 $MgCl_2$, and 10 Na-phosphocreatine, pH 7.2 and 300 mOsm, and $CaCl_2$ was added to reach the appropriate free Ca^{2+} concentration. The amount of total $CaCl_2$ needed to obtain the desired free Ca^{2+} concentration was calculated with Max Chelator (https://somapp.ucdmc.ucdavis.edu/pharmacology/bers/maxchelator/webmaxc/webmaxcE.htm). Final free Ca^{2+} concentration was measured with a Ca^{2+} electrode (Thermo Electron, Beverly, MA) and confirmed our calculations. The extracellular solutions were delivered with the ALA QMM micromanifold perfusion system (ALA Scientific Instrument, Westbury, NY). Recordings were made at room temperature with an Axon 200B amplifier (Axon Instruments, Sunnyvale, CA). Command delivery and data collections were carried out with a Windows-based whole-cell voltage-clamp program, jClamp (Scisoft, Ridgefield, CT), using a Digidata 1322A interface (Axon Instruments). A standard protocol was adopted consisting of stepping the membrane potential from a holding potential of −80 mV to membrane potential 80 mV at 20-mV increments for 100 ms. The clock speed was set at 10 microseconds. Currents were digitized at 100 kHz and filtered at 5–10 kHz. Pipette resistance was ∼3–5 MΩ. Seal resistances for the recordings ranged from 0.5–2 GΩ, (mean 1 GΩ ± 0.06 *SEM*, median 0.8 GΩ, $n = 81$). We corrected for junctional potentials owing to differences in Cl^- concentrations in the pipette and bath solutions. Correction for voltage errors due to the uncompensated series resistance was done offline. Typical values of uncompensated series resistance were ∼10 MΩ. Most of the currents in this manuscript are smaller than 2 nA, so voltage errors would be smaller than 20 mV. Similarly, leak currents were subtracted by estimating linear currents extrapolated from slopes at −95 to −80mV (corrected) where currents were linear. The average leakage current between these voltages was 0.035 nA (±0.002 *SEM*).

$V_{1/2}$ values were calculated from conductance–voltage (G–V) curves. Normalized G–V curves were obtained

by calculating the conductance of averaged amplitudes of currents at steady state after depolarization to various test voltages from holding the cells at −80 mV. Conductance (G) was derived from Hodgkin and Huxley (1952) and normalized (G/Gmax) to derive relative conductance to voltage relationships.

$$G = I/(V - V_K)$$

where G is the conductance, V is the step voltage, V_K is the equilibrium potential for K^+ (calculated to be −122 mV), and I is the current at that step voltage.

Each *G–V* curve was fitted with a Boltzmann function:

$$G(V) = \frac{G_{max}}{1 + \exp^{\frac{-zF(V-V_h)}{RT}}}$$

where G_{max} is the fitted value for maximal conductance, V_h is the voltage of half-maximal activation of conductance, and z reflects the net charge moved across the membrane during the transition from the closed to the open state. Data are reported as mean ± *SEM*.

2.2 | Calcium imaging with confocal microscopy

Imaging was performed of chick hair cells from freshly isolated basilar papilla from E21 chicks as previously described for a chloride sensor developed in our lab (Zhong, Navaratnam, & Santos-Sacchi, 2014; Zhong et al., 2019). Chick hair cells were incubated with 1 μM Fluo-3-AM for 30 min at 22–24°C. Stock solutions of 1 mM Fluo-3-AM in DMSO were diluted to 1 μM in aqueous solution. Typically, cells were incubated in the presence of artificial perilymph (in mM: 144 NaCl, 0.9 $MgCl_2$, 1.3 $CaCl_2$, 0.7 NaH_2PO4, 10 HEPES, and 5 glucose, pH 7.4 and 300 mOsm). Perilymph containing 1 μM Fluo-3-AM was substituted with perilymph at the time of fluorescence measurement. In experiments with nominally 0 μM Ca^{2+}, $CaCl_2$ was removed and 2 mM EGTA added with the remaining constituents of the perilymph solution remaining constant. The papilla was mounted on a glass microtek dish under two insect pins, and Ca^{2+} signal was visualized while exciting at 488 nm using a Zeiss inverted spinning disc confocal microscope (Zeiss Observer Z1) with a 40X objective using 0.4-μm optical sections. For control experiments, hair cells were incubated with medium containing specific concentrations of Ca^{2+} in the presence of the Ca^{2+} ionophore A23187 (1 μm) and 1 μM Fluo-3-AM for 30 min at 22-24°C (Dedkova, Sigova, & Zinchenko, 2000). Where we measured effects of drugs in a time-dependent manner, fluorescence from the same cells was tracked with the focal plane unchanged. Drift correction was applied to compensate for specimen drift. Image data were quantified with background correction using Zeiss Zen and Fiji software.

2.3 | Statistical analysis

Standard statistical analysis (*t* test, ANOVA) was performed using the statistical tools included in Prism 7 software (Graphpad Software).

For experiments where effects of extracellular solution changes by perfusion were measured, two-tailed paired *t* tests were performed on each of the paired datasets. Where different concentrations of intracellular or buffers were compared or where effects of drugs affecting CICR on intracellular Ca^{2+} were measured, ANOVA with multiple comparison tests between groups was used. For comparison of the size of currents with drug treatments we compared the size of the measured current at a specific voltage (typically at peak current in the pretreatment group).

2.4 | Stochastic optical reconstruction microscopy (STORM) microscopy

Chick basilar papilla was labeled following protocol for super-resolution microscopy. In brief, freshly isolated basilar papillae were isolated and hair cells exposed by removal of the tectorial membrane following treatment with 0.5% collagenase for 4–5 min. Tissue was preextracted with 0.2% saponin followed by a fixation with 3% PFA and 0.1% glutaraldehyde. The tissue was reduced with 0.1% NaBH and labeled with primary (1:50) and secondary antibody (1:400, donkey anti-mouse Alexa 647 and donkey anti-rabbit Alexa 561) after blocking, with three washes of 3 min each between each step. The sample was post-fixed after antibody labeling with 4% PFA for 5 min. Freshly made imaging buffer containing glucose oxidase, catalase, mercaptoethanol, and MEA was added just before imaging. Super-resolution STORM images were obtained with the Bruker Vutara SR352 (Bruker Nano Surfaces, Salt Lake City, UT) with a 60x 1.2 NA objective and a 1 W 561-nm and 640-nm laser. Imaging beads confirmed that resolution was 20 nm in the *xy* plane and 50 nm in the *z*-direction. Calibration before experimentation was done by calculating the point spread function (PSF) in three dimensions using beads. Images were rendered and analyzed with Vutara's SRX localization and visualization software (v6.2). Images were obtained in both planes simultaneously. The background was removed after the frames were obtained and particles identified on their brightness. Three-dimensional localization of the particles was based on 3D model function that was obtained from recorded bead datasets. The recorded fields are aligned automatically by computing the affine transformation between the pair of planes. Typically, we collected 5,000 frames with each fluorophore using 20 μsec times. Data were analyzed using algorithms embedded

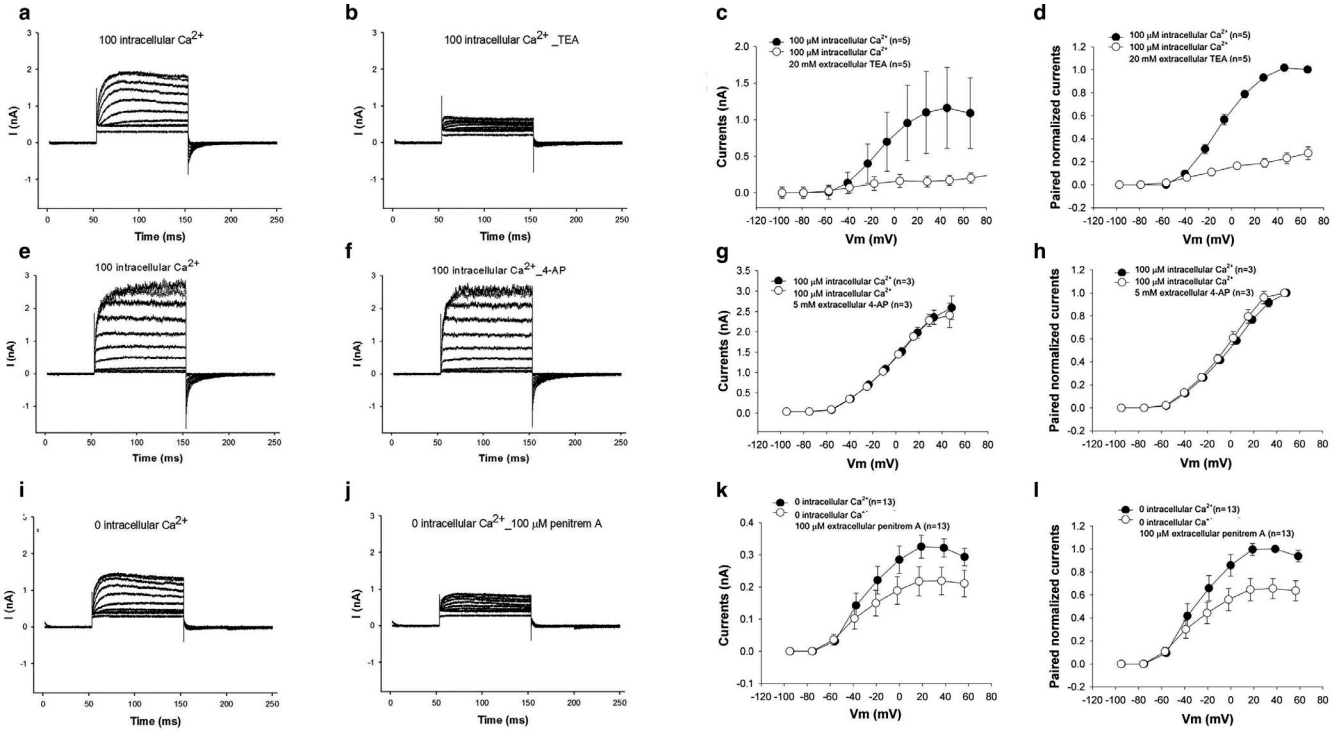

FIGURE 1 Hair cells have a large outward potassium current. a–d. The outward current is reduced by the application of extracellular 20mm TEA. Shown are individual representative current recordings of a cell under voltage clamp before (a) and after (b) perfusion with extracellular TEA. Averaged I–V relationships (c) and paired averaged currents normalized to preperfusion currents (d) of cells perfused with TEA shows a 75% reduction in the size of the current with TEA perfusion These differences in averaged current (c) before and after perfusion were statistically significant ($p < .05$, paired t test, $n = 5$). (e–h) The size of the current is unaffected by 100 μM 4AP. Shown are representative current recordings of an individual cell before (e) and after perfusion (f) with 4-AP. Averaged I–V relationships (g) and paired averaged currents normalized to preperfusion currents (h) of cells perfused with 4AP show no change in the size of the current with 4AP perfusion. (i–l) The differences in averaged current (g) before and after perfusion were statistically not significant ($p > .05$, paired t test, $n = 3$). The size of the current is partially reduced by 100 μM of penitrem A, a partial inhibitor of BK channels. Representative current recordings of cells under voltage clamp before (i) and after (j) perfusion with 100 μM Penitrum A. Averaged I–V relationships (k) and paired averaged currents normalized to preperfusion currents (l) of cells perfused with penitrum A show a moderate reduction in the size of the current with penitrum A perfusion. These differences in averaged currents (k) before and after perfusion were statistically significant ($p < .05$, paired t test, $n = 13$)

in the Vutura software. These include the crossed nearest neighbor algorithm and cluster identification. All chemicals were purchased from Sigma-Aldrich. Primary antibodies were as follows: mouse IgG2a monoclonal anti-BK channel α subunit antibody (BD Labs) (Surguchev, Bai, Joshi, & Navaratnam, 2012), anti-BK channel α subunit polyclonal antibody (APC021) (Alomone labs, Jerusalem, Israel) (Purcell, Liu, Thomas, & Duncan, 2011); IgG1 monoclonal anti-ryanodine receptor antibody (clone 34C, Developmental Studies Hybridoma Bank, University of Iowa, Iowa City, Iowa; this antibody detects all RyR isoforms in mouse tissue) (Irie & Trussell, 2017); rabbit polyclonal anti IP3R2 antibody (Alomone labs, Jerusalem, Israel) (Sabourin et al., 2018; Tadevosyan et al., 2017). Secondary antibodies were as follows: AF 568 goat anti-mouse IgG, AF 568 goat anti-rabbit IgG, Alexa Fluor 647 goat anti-rabbit IgG, and Alexa Fluor 647 goat anti-mouse IgG (Jackson labs, Maine). We used mouse monoclonal Slo antibody with the polyclonal rabbit IP3 antibody (and corresponding conjugated secondary antibodies) to detect co-localization of these two proteins. For experiments to detect ryanodine receptor and Slo protein, we used the Slo polyclonal rabbit antibody and ryanodine monoclonal mouse antibody together with the corresponding secondary antibodies. All primary antibodies were used at a concentration of 1μg/ ml. All secondary antibodies were used at a 1:200 dilution. These antibodies have all been previously validated.

3 | RESULTS

3.1 | Hair cells possess a BK current that is sensitive to entry of extracellular Ca^{2+}, and intracellular Ca^{2+} buffering

Current recordings of chick hair cells from the neural edge, 20%–25% of the distance of the basilar papilla from the apical end, were obtained under whole-cell voltage-clamp conditions. We confirmed the location of these hair cells using stereociliary height (Tilney et al., 1986). As previously

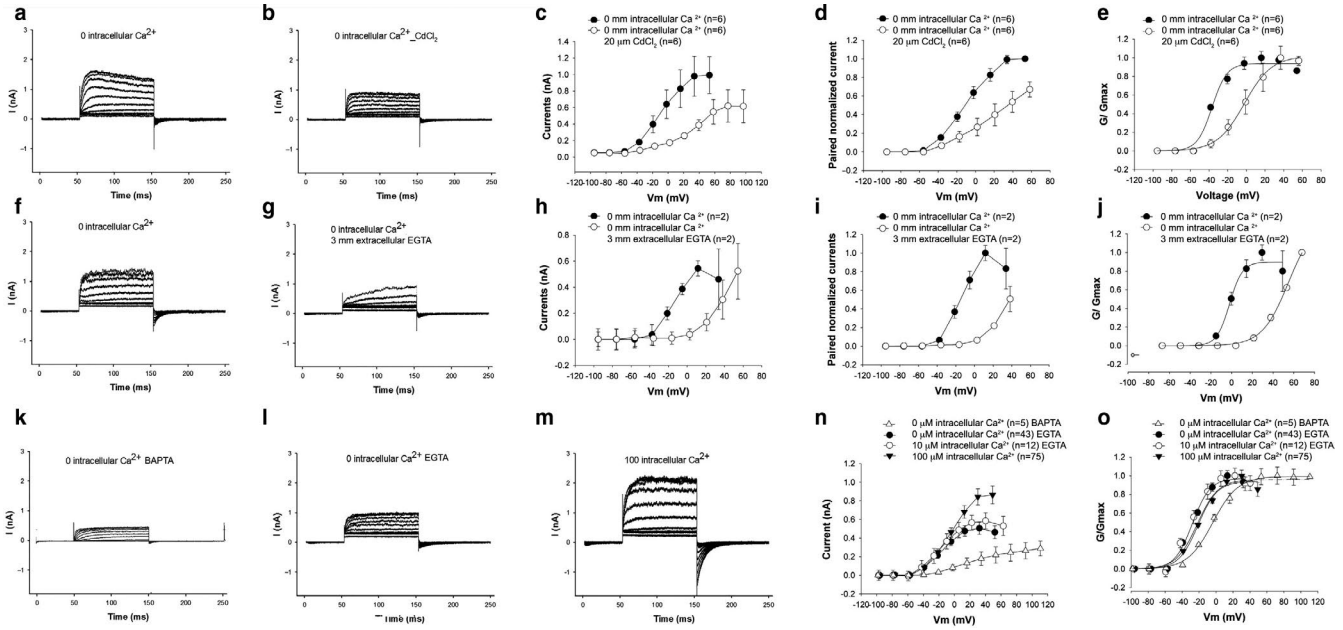

FIGURE 2 Hair cell BK currents are dependent on extracellular Ca^{2+} and intracellular Ca^{2+} buffer that have similar effects. (a–e) Extracellular $CdCl_2$ reduces the size of the outward current. Representative current recordings of hair cells under voltage clamp before (a) and after (b) perfusion of 20 µM $CdCl_2$ into the extracellular bath solution. Averaged I–V relationships (c) and paired averaged currents normalized to preperfusion currents (d) of cells perfused with $CdCl_2$ shows a 60% reduction in the size of the current at comparable voltages with $CdCl_2$ perfusion. These differences in averaged currents (c) before and after perfusion were statistically significant ($p < .05$, paired t test, $n = 13$). Currents are also significantly shifted in a depolarizing direction after perfusion (e**,** $p < .001$**,** paired t test, $n = 13$). (f–j) A similar effect is seen with reducing extracellular Ca^{2+}. Shown are representative current recordings of hair cells under voltage clamp before (f) and after (g) perfusing with bath solution containing 3 mM EGTA. Averaged currents (h) and averaged paired currents normalized to currents before perfusion (i) show a reduction in the size of the currents with EGTA perfusion. Currents show a 51 mV depolarizing shift in its conductance-voltage relationship after reducing the extracellular Ca^{2+} concentration (j). We had difficulty maintaining seal resistance with EGTA perfusion and were unable to record more than 2 cells that did not permit statistical validation, but believe the data to be valid given the degree of shift in voltage. (k–o) Specific buffers and intracellular Ca^{2+} variably affect the size of the current and its normalized (g–v) relationship**.** Shown are representative current recordings of hair cells under voltage clamp with nominally 0 µM Ca^{2+} buffered with BAPTA in the pipette (k), nominally 0 µM Ca^{2+} buffered with EGTA in the pipette (l) and 100 µM Ca^{2+} in the pipette (m). Averaged currents (n) show a reduction in the size of the currents with reducing intracellular Ca^{2+} that was especially marked with greater spatial buffering afforded by BAPTA (0 µM Ca^{2+}). The differences in peak currents were statistically significant (ANOVA multiple comparison: $p < .05$, for BAPTA versus. 10 µM Ca^{2+}, $p < .01$ BAPTA versus. 100 µM Ca^{2+}, $n = 5$ (BAPTA, 0 µM Ca^{2+}), 43 (EGTA, 0 µM Ca^{2+}), 10 (EGTA, 10 µM, Ca^{2+}) 75 (EGTA, 100 µM Ca^{2+}). Currents show a depolarizing shift in its conductance-voltage relationships with greater spatial buffering provided with BAPTA (**o**). The differences in $V_{½}$ were statistically significant (ANOVA multiple comparison, $p < .01$, for BAPTA versus 0 µM (EGTA) and 10 µM Ca^{2+}(EGTA), $p < .05$ BAPTA versus 100 µM Ca^{2+} (EGTA), $n = 5$ (BAPTA, 0 µM Ca^{2+}), $n = 43$ (EGTA, 0 µM Ca^{2+}), $n = 10$ (EGTA, 10 µM, Ca^{2+}), $n = 75$ (EGTA, 100 µM Ca^{2+}))

demonstrated (Fuchs & Evans, 1990; Fuchs, Nagai, & Evans, 1988) (Fuchs & Sokolowski, 1990), these cells demonstrated a large outward current with 140 mM KCl in the pipette and 140 mM NaCl in the bath (Figure 1a). Consistent with previous experimental data, the majority of the current was carried by a large-conductance Ca^{2+}-activated K channel (Duncan & Fuchs, 2003; Fuchs & Evans, 1990; Fuchs et al., 1988; Fuchs & Sokolowski, 1990). The outward current showed rapid rates of activation that is a hallmark of BK currents. Consistent with it being a BK current, it was blocked by extracellular TEA (20mM), partially blocked by 100 µM penitrem A, an incomplete blocker of BK channels, and insensitive to 5mM 4-AP, a blocker of voltage-gated potassium channels (Figure 1a–i). The bath also contained 100 µM linopirdine, 300 nM apamin and 50 µM PPADS, blockers of KCNQ and SK channels and P2 purinergic receptors, respectively, the other sources of outward currents in these cells. As previously reported, these BK current are insensitive to charybdotoxin and iberiotoxin owing to the high expression of the beta4 (KCNMB4) subunit that confers resistance to these blockers (Bai et al., 2012a; Brenner et al., 2005; Brenner, Jegla, Wickenden, Liu, & Aldrich, 2000; Gan et al., 2008; Meera, Wallner, & Toro, 2000; Reinhart, Chung, & Levitan, 1989).

The size of the outward current and its voltage sensitivity was dependent on the inward flow of Ca^{2+}. The size of the current decreased and showed a rightward shift in its voltage-current relationship when voltage-gated Ca^{2+} channels were blocked with 100 µM $CdCl_2$ (Figure 2a–e). $V_{½}$ (calculated from normalized G–V curves) was shifted significantly

from −37 mV to −2 mV after perfusion with $CdCl_2$. There was a similar marked 51 mV shift in $V_{1/2}$ from −21 mV to 32 mV (again calculated from normalized G–V curves) and a reduction in the size of the current (Figure 2f–j) when extracellular Ca^{2+} was chelated (with 3 mM EGTA).

The size and voltage dependence of the current is dependent on the intracellular Ca^{2+} buffer (Figure 2k–o). The voltage dependence was significantly shifted in a depolarizing direction when using BAPTA as the intracellular buffer (with nominally 0 μM Ca^{2+}) compared to using EGTA as the intracellular buffer (again, with nominally 0 μM Ca^{2+}). $V_{½}$ was shifted significantly from −27 mV to −4 mV with EGTA and BAPTA as the intracellular buffers, respectively ($V_{½}$ was estimated from normalized G–V curves). The size of the outward current was also reduced when BAPTA (nominally 0 μM Ca^{2+}) was used as the intracellular buffer when compared to using intracellular EGTA (nominally 0 μM Ca^{2+}). These data argue that spatial buffering by BAPTA significantly attenuates influx of Ca^{2+} in proximity to BK channels. It has been estimated that buffering by BAPTA limits the spread of Ca^{2+} to 20–50 nm (nanodomains). In contrast, owing to the slower on rate of EGTA spatial buffering is limited to micro-domains (> 50 nm) (Augustine, Santamaria, & Tanaka, 2003; Heidelberger, Heinemann, Neher, & Matthews, 1994; Neher, 1998).

Increasing intracellular Ca^{2+} in the presence of EGTA from 0 to 10 μM resulted in an increase in the size of the current (Figure 2k–o). The size of the current was further significantly increased in the presence of 100 μM Ca^{2+} ($p < .02$, ANOVA multiple comparison test 0 and 100 μM Ca^{2+}; $p > .05$ for both 0 μM Ca^{2+} and 10 μM Ca^{2+}, and 10 μM Ca^{2+} and 100 μM Ca^{2+}). However, these increases in the size of the current were accompanied by a minimal shift in voltage sensitivity with $V_{1/2}$ ranging from −29 mV to −21 mV (Figure 2k–o, $p > .05$, ANOVA multiple comparison test). Along with the data from recordings in the presence of BAPTA, these data argue that the local concentration of Ca^{2+} in proximity to BK channels from inward flow of Ca^{2+} is spatially buffered by BAPTA. They also argue that the local concentration of Ca^{2+} around BK channels is saturating in the presence of EGTA with nominally 0 μM and higher Ca^{2+} (when spatial buffering is more limited). Finally, these data suggest that spatial buffering of intracellular Ca^{2+} is a possible mechanism of recruiting BK channels.

3.2 | Perfusion with activators of PKA increased the size of the outward current

Perfusing cells with 100 μM forskolin increased the size of the outward current by twofold (Figure 3a–c), an effect similar to increasing intracellular (pipette) Ca^{2+} (Figure 2). The effect of forskolin was dependent on the concentration of intracellular Ca^{2+}. Thus, the forskolin-induced increase in outward current was evident with 100 μM intracellular (pipette) Ca^{2+} with EGTA (Figure 3a–e). In contrast, there was no increase in the size of the current in the presence of nominally 0 μM intracellular (pipette) Ca^{2+} with EGTA (Figure 3f–j). The effects of forskolin in the presence of 10 μM Ca^{2+} was intermediate (data not shown). $V_{1/2}$ was affected, shifting a nonsignificant −5 mV to –17 mV with forskolin (with 100 μM pipette Ca^{2+}). Confirming a basal activation of PKA in hair cells contributing to BK channel activity, with 100 μM Ca^{2+} in the pipette, perfusion of the PKA inhibitor H-89 reduced the size of the outward current by approximately 1/3 (Figure 3k–o). This reduction in the size of the current was not accompanied by a change in the voltage-current relationship (Figure 3k–o). $V_{½}$ was shifted by a nonsignificant −18 mV to −15 mV after perfusion with H-89. Together, these data suggest that PKA increases BK channel activity that is dependent on intracellular Ca^{2+} concentration and that hair cells have a basal level of PKA activity.

3.3 | The effects of forskolin on the outward current are due to Ca^{2+}-induced Ca^{2+} release

How does PKA increase BK channel activity while minimally affecting $V_{1/2}$? Direct effects on the channel bearing the STREX exon (the dominant exon in these hair cells) would be predicted to shift $V_{1/2}$ in a depolarizing direction (Frucht et al., 2011; Tian et al., 2001). Since forskolin effects on hair cell outward current were dependent on pipette Ca^{2+} concentration, Ca^{2+}-induced Ca^{2+} release was suggested as a likely mechanism. To test this possibility, we treated cells with an inhibitor of ryanodine receptors. Currents from hair cells under voltage clamp were recorded in the presence of 100 μM pipette Ca^{2+} and cells treated with 10 μM dantrolene, a potent blocker of ryanodine receptors (Figure 4f–j). There was a significant reduction in the size of the current. The reduction in the size of the current was also not accompanied by a change in its voltage dependence. $V_{1/2}$ shifted in a nonsignificant fashion from −20 mV to −29 mV. Separately, cells treated with 10 μM dantrolene and 100 μM forskolin showed a similar reduction in the size of the outward current (Figure 4a–e). Here too $V_{1/2}$ shifted from −16 mV to a statistically insignificant −26 mV after treatment.

We also tested the ability of inhibitors of IP3 receptors (ITPRs) to block the effects of forskolin. Similar to dantrolene, cells treated with the IP3 receptor antagonist 100 μM 2-APB (2-aminoethoxydiphenyl borate), show a similar reduction in the size of the outward current (Figure 5f–h). The voltage sensitivity shifted in a depolarizing direction with $V_{1/2}$ shifting from −21 mV to −12 mV. As with dantrolene and forskolin, hair cells separately treated with 100 μM 2-APB and 100 μM forskolin showed a significant decrease in the size of the outward current (Figure 5a–e). Unlike dantrolene, however, there was a greater reduction

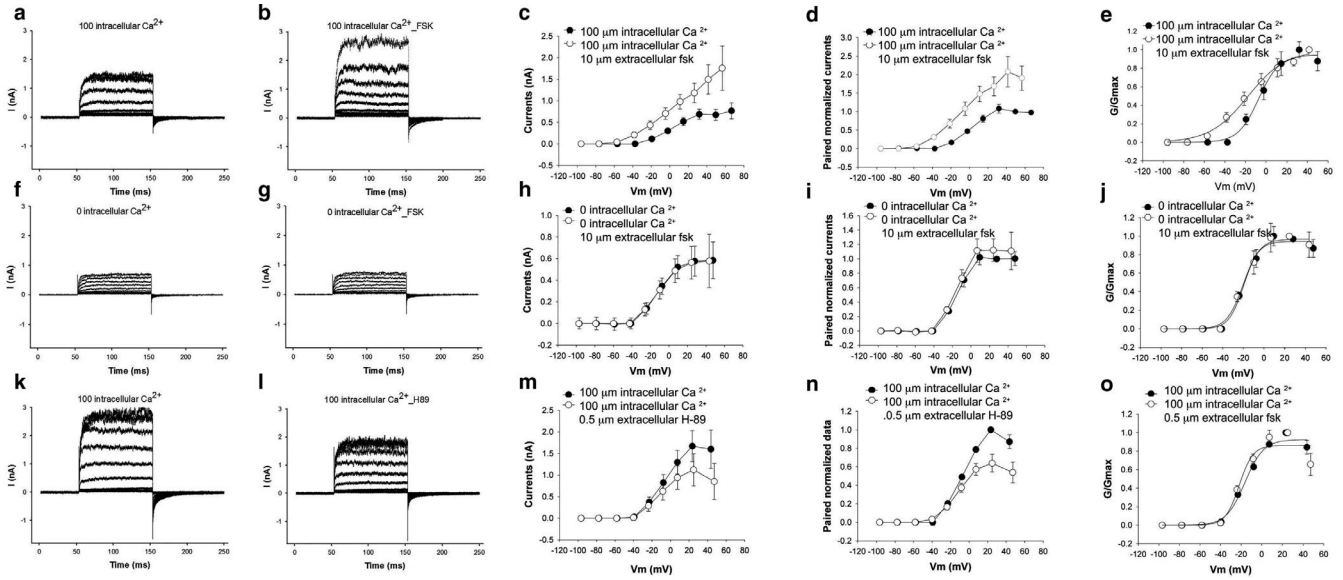

FIGURE 3 Forskolin increased the size of the outward current in a Ca^{2+}-dependent manner. (a–c) Representative current recordings of hair cells before (a) and after (b) perfusion with 100 μM forskolin with the pipette containing 100 μM Ca^{2+}. The size of the outward current increased twofold when hair cells were perfused with 100 μM forskolin evidenced in averaged currents (c), and averages of pre and post perfusion paired currents normalized to pre perfusion currents (d). The differences in the sizes of currents (c) was significant ($p < .01$, paired t test, $n = 9$). Currents also show a hyperpolarizing shift in voltage sensitivity that was however, not statistically significant (e, $p > .05$, paired t test, $n = 9$). (f–k) In contrast, perfusion of hair cells with 100 μM forskolin with nominally 0 μM pipette Ca^{2+} (with EGTA as the intracellular buffer) did not cause an increase in the size of the current or a change in its conductance–voltage relationship. Shown are representative current recordings of hair cells under voltage clamp before (f) and after (g) perfusion with 100 μM forskolin. The averaged I–V relationship of cells before and after perfusion with forskolin compared to pre perfusion (h) and paired averaged currents from individual cells normalized to values before perfusion (i) confirm an absence of an effect on the size of the current. G–V curves (j) to elicit voltage relationships do not show an effect on its normalized G–V relationship. Neither the change in currents or G–V relationships was significant ($p > .05$, paired t test, $n = 10$). (k–o) Perfusion of hair cells with 0.5 μM H-89, a well-known PKA blocker resulted in a reduction in the size of the current. Representative current recordings of cells under voltage clamp before (k) and after (l) perfusion with H-89 are shown. The averaged I–V relationships of cells before and after perfusion with H-89 (m) and averaged currents from individual cells pre and post perfusion normalized to values before perfusion (n) confirm a 30% decrease in the size of the currents with H-89. The decrease in the size of the current was statistically significant ($p < .05$, paired t test, $n = 7$). Normalized G–V curves (o) to elicit voltage relationships show a nonsignificant change in voltage sensitivity ($p > .05$, paired t test, $n = 7$)

in the size of the current when 2-APB was combined with forskolin (when compared to 2-APB alone). Currents were 40% of preperfusion values with 2APB and forskolin, in contrast to the effects of 2APB alone where currents were 66% of preperfusion values. Moreover, there was a significant depolarizing shift in the $V_{1/2}$ from −36 mV to −6 mV. We believe these effects on the size of the current and its normalized G–V relationship to represent two causes; a reduction in local Ca^{2+} concentrations by preventing CICR, and a directly inhibitory effect of PKA on the Slo channel containing the STREX exon in the absence of local release of Ca^{2+} (Chen et al., 2005; Frucht et al., 2011; Ramanathan et al., 2000). Although these experiments were not specifically designed to address the concern of effects at a hair cells operating voltage, we noted that IP3 receptor blocking had a significant effect on the size of the outward current at a hair cells operating voltage, estimated to be −50 mV, in contrast to block of ryanodine receptors.

Together, these data confirm that PKA increases hair cell Ca^{2+} concentration in proximity to BK channels by a CICR mechanism, with inhibition of IP3 receptors having a bigger effect than inhibition of ryanodine receptors.

3.4 | Ca^{2+} imaging reveals clusters of Ca^{2+}signal in the periphery of hair cells that is dependent on CICR

To confirm Ca^{2+} influx and its effects, we imaged hair cells loaded with the Ca^{2+} sensor dye Fluo-3-AM. We noted a significant increase in the Fluo-3 signal when the cells were incubated with perilymph that contains 1.3 mM Ca^{2+}. The signal was most notable along the periphery of the cell in axial sections when the cell was viewed end-on from above (Figure 6a). In cells viewed laterally, there was a significant increase in signal at the periphery of the cell that was weighted to the lower half of the cell (Figure 6c). In contrast, cells kept in nominally 0 μM extracellular Ca^{2+} showed no peripheral increase in Ca^{2+}signal (Figure 6b).

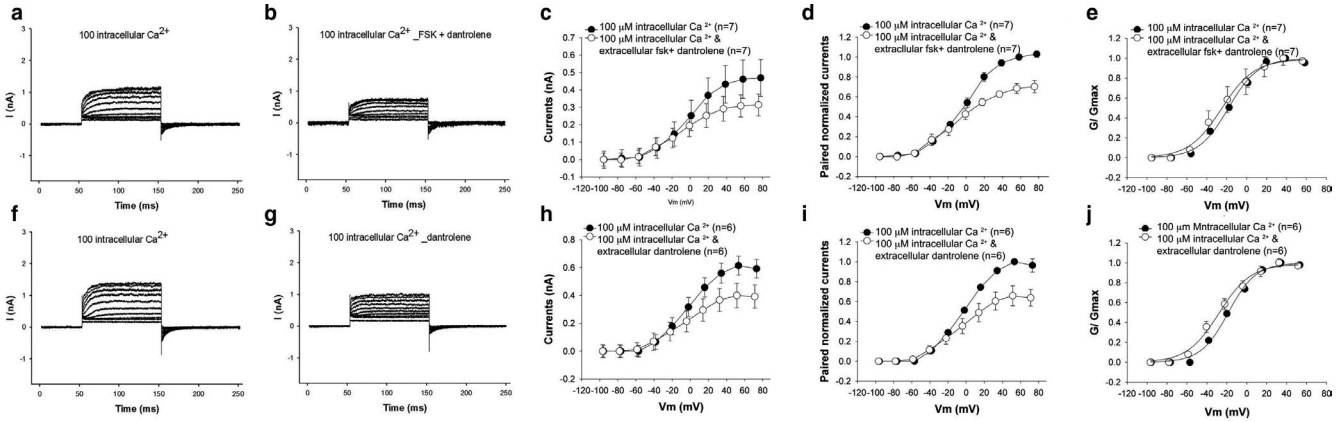

FIGURE 4 Blocking ryanodine receptors prevents a forskolin-induced increase in the outward current. (a–e) The I–V relationship of the outward current before and after perfusion with 100 μM forskolin and 1 μM Dantrolene shows a decrease in the size of the current with no change in the I–V relationship. The pipette contained 100 μM $Ca2^{+}$. Shown are representative current recordings of cells under voltage clamp before (a) and after (b) perfusion with forskolin and dantrolene. Averaged currents (c) and averaged currents of pairs of currents before and after perfusion normalized to preperfusion currents (d) show an approximately 33% reduction in current in cells treated with both dantrolene and forskolin. The reduction in the size of the current (c) was statistically significant ($p < .05$, paired t test, $n = 7$). Normalized G–V curves (e) show no change in voltage sensitivity ($p > .05$, paired t test, $n = 7$). (f-j) A similar reduction (27%) in the size of the current with no change in the I–V relationship is seen when hair cells are perfused with 1 μM Dantrolene alone without forskolin. Here too, the pipette contained 100 μM Ca^{2+}. Shown are representative current recordings of cells under voltage clamp before (**f**) and after (g) perfusion with dantrolene. The averaged currents (h) and averaged currents of pairs of currents before and after perfusion normalized to prepefusion currents (i) show a reduction in the size of the current after perfusion with dantrolene. The reduction in the size of the current (h) was significant ($p < .05$, paired t test, $n = 6$). Here too, the reduction in the size of the current was approximately 1/3 indicating that the addition of forskolin had no additional effect in the presence of dantrolene. Normalized G–V curves (j) show no change in voltage sensitivity ($p > .05$, paired t test, $n = 6$)

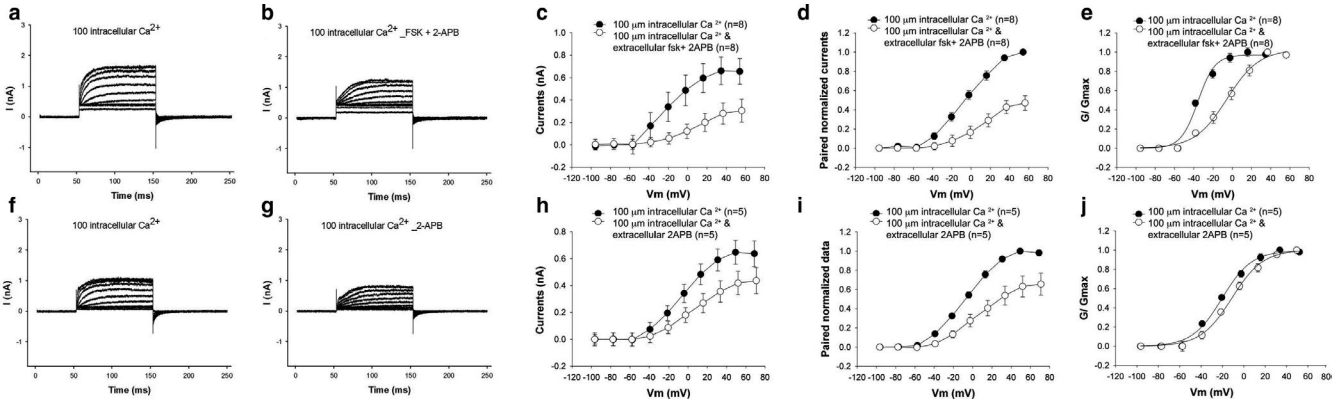

FIGURE 5 Blocking IP3 receptors prevents a forskolin-induced increase in the outward current. (a-e) The I–V relationship of the outward current before and after perfusion with 100 μM forskolin and 100 μM 2-APB shows a larger decrease in the size of the current. The pipette contained 100 μM Ca^{2+}. Shown are representative current recordings of cells under voltage clamp before (a) and after (b) perfusion with forskolin and dantrolene. Averaged currents (c) and averages of paired currents before and after perfusion normalized to preperfusion currents (averaged currents of pairs of currents before and after perfusion (d)) demonstrate current values to be 40% of the current before perfusion with 2-APB and forskolin. The reduction in current (c) was significant ($p < .02$, paired t test, $n = 8$). Normalized G–V curves (e) show a significant shift in voltage sensitivity in cells treated with forskolin and 2-APB ($p < .05$, paired t test, $n = 8$). (f–j) A smaller reduction in the size of the current with a change in the I–V relationship is seen when hair cells are perfused with 100 μM 2-APB alone without forskolin. Here too, the pipette contained 100 μM Ca^{2+}. Shown are representative current recordings of cells under voltage clamp before (f) and after (g) perfusion with 100 μM 2-APB. Averaged currents (h) and averages of paired currents before and after perfusion normalized to preperfusion currents (i)) show a smaller 1/3 decrease in the size of the current when cells were perfused with 2-APB alone. The differences in current (h) were statistically significant ($p < .05$, paired t test, $n = 5$). Normalized G–V curves (j) show a small shift in voltage sensitivity after perfusion with 2-APB ($p > .05$, paired t test, $n = 5$)

In contrast to the peripheral accumulation of signal in hair cells incubated with perilymph alone, the addition of inhibitors of both IP3 receptors (10 μM 2-APB) and ryanodine (100 μM dantrolene) resulted in a marked reduction in the intensity of Ca^{2+} signal (Figure 7). These findings were reflected in the gradient in peripheral Ca^{2+}

signal that was significantly attenuated in the presence of these two inhibitors (Figure 7). We conclude that peripheral Ca^{2+} signal in hair cells is increased by physiological concentrations of extracellular Ca^{2+} that in turn induces local CICR.

3.5 | 8-BR-camp increases the local Ca^{2+} concentration, particularly at the periphery of the cell

We determined the effects of raising cAMP levels while monitoring intracellular Ca^{2+}. Figure 8 shows the effects of 100 μM 8-br-cAMP, the cell-permeable analog of cAMP that activates PKA, on intracellular Ca^{2+} concentration. We note a spike in Ca^{2+} concentration that followed treatment with 8-br-cAMP (Figure 8). The increase in Ca^{2+} signal was most notable along the periphery of the cell. In contrast, cells pretreated with 100 μM dantrolene and 100 μM 2-APB showed minimal to no increase in the size of the Ca^{2+} signal. Since the Ca^{2+} signal was significantly attenuated, and particularly along the periphery of the cell, by treating with IP3 and ryanodine antagonists, we used the Ca^{2+} signal in the entire cell for these comparisons. These data confirm that PKA activation increases peripheral Ca^{2+} concentrations by CICR.

3.6 | We made estimates of Ca^{2+} concentration in hair cells incubated in bath solution that approximated that of perilymph

Our cumulative data suggest a high concentration of Ca^{2+} in proximity to BK channels in the experimental conditions we used for our electrophysiological recordings. Prior work has demonstrated BK channels to lie in proximity to VGCCs at the periphery of the cell (Issa & Hudspeth, 1994; Roberts et al., 1990; Samaranayake, Saunders, Greene, & Navaratnam, 2004). We sought to determine the concentration of Ca^{2+} along the periphery of the cell in the presence of perilymph. For these experiments, we calibrated the Ca^{2+} fluorescence by using the Ca^{2+} ionophore A23187 and incubated cells in different concentrations of external Ca^{2+} for 30 min before measuring Ca^{2+} signal (Dedkova et al., 2000). In Figure 9, we determine the concentration of Ca^{2+} along the periphery of hair cells incubated in perilymph to be in excess of 100 μM. These data are in broad agreement with our electrophysiological data suggesting

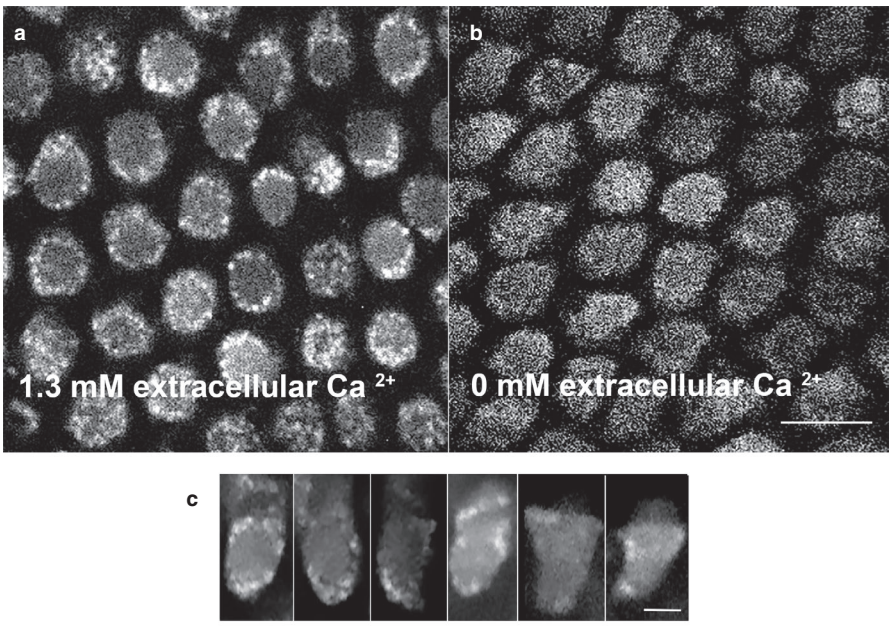

FIGURE 6 In artificial perilymph, hair cells show high concentrations of peripheral Ca^{2+} in clusters. (a) Hair cells viewed end-on from above using confocal microscopy show high concentrations of peripheral Ca^{2+}. Ca^{2+} was detected after incubating cells in 1 μM Fluo-3-AM in perilymph containing 1.3 mM Ca^{2+}. These high concentrations of Ca^{2+} are not uniformly spread along the periphery and are clustered. (b) Hair cells incubated with 1 μM Fluo-3-AM in perilymph containing nominally 0 μM Ca^{2+} for 30 min at room temperature are viewed end-on from above and show absent peripheral concentration of Ca^{2+} signal. Scale bar = 10 μm. (c) Hair cells in basilar papillae incubated with 1 μM Fluo-3-AM in perilymph for 30 min at room temperature viewed side on show high concentrations of peripheral Ca^{2+}. Here too, the Ca^{2+} signal is clustered. Also, note increased signal in stereocilia and in the region of the cuticular plate. Scale bar = 5 μm

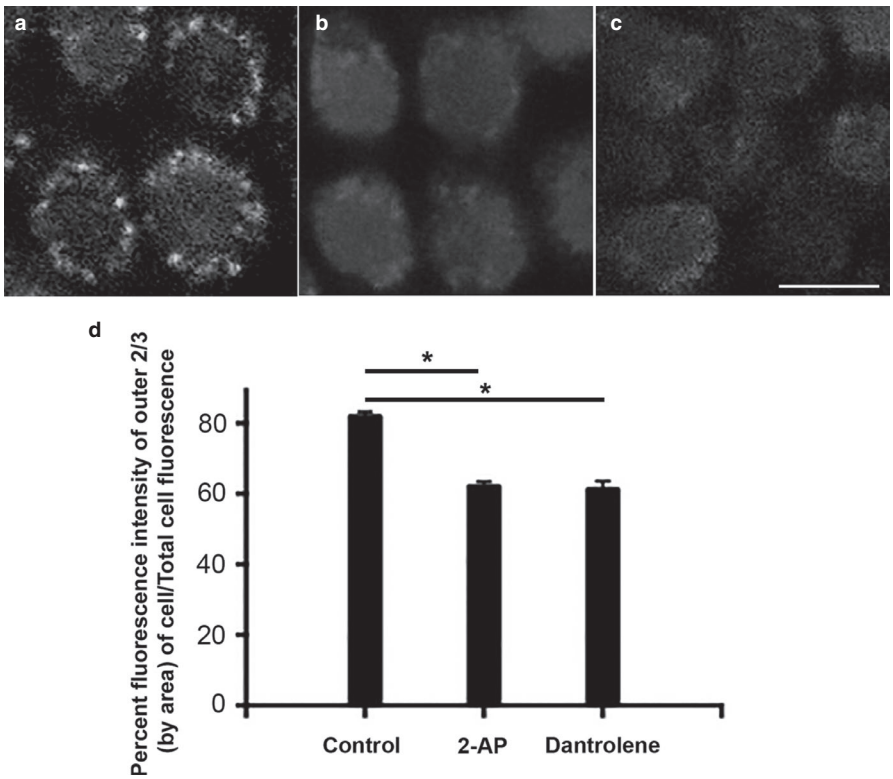

FIGURE 7 In perilymph, hair cells do not show high concentrations of peripheral Ca^{2+} in the presence of inhibitors of CICR. (a) Control cells incubated in 1 μM Fluo-3-AM in perilymph (1.3 mM Ca^{2+}) for 30 min shows a peripheral accumulation of Ca^{2+} along the periphery of the cell. Data were acquired using a spinning disc confocal microscope with the cells viewed end on from above. (b, c) Addition of 100 μM 2-APB (b) or 1 μM dantrolene (c) both prevent an increase in the peripheral accumulation of Ca^{2+}. (d) These effects of inhibitors of CICR were quantified. Shown is the cumulative Ca^{2+} signal in the peripheral 2/3 of the cell viewed end-on. In the presence of inhibitors of CICR, there is a significant reduction in the accumulation of peripheral Ca^{2+} signal as a percentage of the signal in the entire cell ($p < .01$, one-way ANOVA, $n = 10$ cells). Scale bar = 5 μm

local concentrations of Ca^{2+} in excess of that required to activate BK channels.

3.7 | The Slo channel clusters with both IP3 and ryanodine receptors along the periphery of the cell where they lie within a hundred nanometers of each other

Since hair cells contain high concentrations of Ca^{2+} buffer that are thought to provide significant spatiotemporal buffering, we sought to determine the localization of IP3 receptors and ryanodine receptors in hair cells in relationship to BK channels. For these experiments, we localized Slo, the BK alpha subunit, a key constituent of the BK channel complex, and the IP3 receptor using immunolabeling. We used STORM/ PALM super-resolution microscopy for these experiments. As shown in Figure 10, both these proteins were localized along the periphery of the cell. The proteins were clustered in close proximity with one another along the periphery of the cell. In most clusters, we noted the proteins to lie in apposition in the 2D plane, or when separated to lie less than a hundred nanometers of one another. We see a similar distribution with clustering and close proximity between the Slo channel and ryanodine receptors. Here too, the proteins are closely positioned and lie within nanometers from one another along the periphery of the cell (Figure 10). Using the nearest neighbor algorithm, we determine that the Slo channels lie as close as 5 nm from IP3 receptors with peak distances between these proteins between 55 and 85 nm (Figure 11). Similarly, Slo channels and ryanodine receptors lie as close as 15 nm apart with the peak distribution of distances between Slo and ryanodine receptors between 85 and 135 nm (Figure 11). These data support the presence of nanodomains within these cells, similar to that in cartwheel inhibitory interneurons of the dorsal cochlear nucleus (Irie & Trussell, 2017). The super-resolution data are concordant with our electrophysiological and Ca^{2+} imaging data.

4 | DISCUSSION

In this paper, we show for the first time the effects of CICR on BK channel function in hair cells of the chicken. We

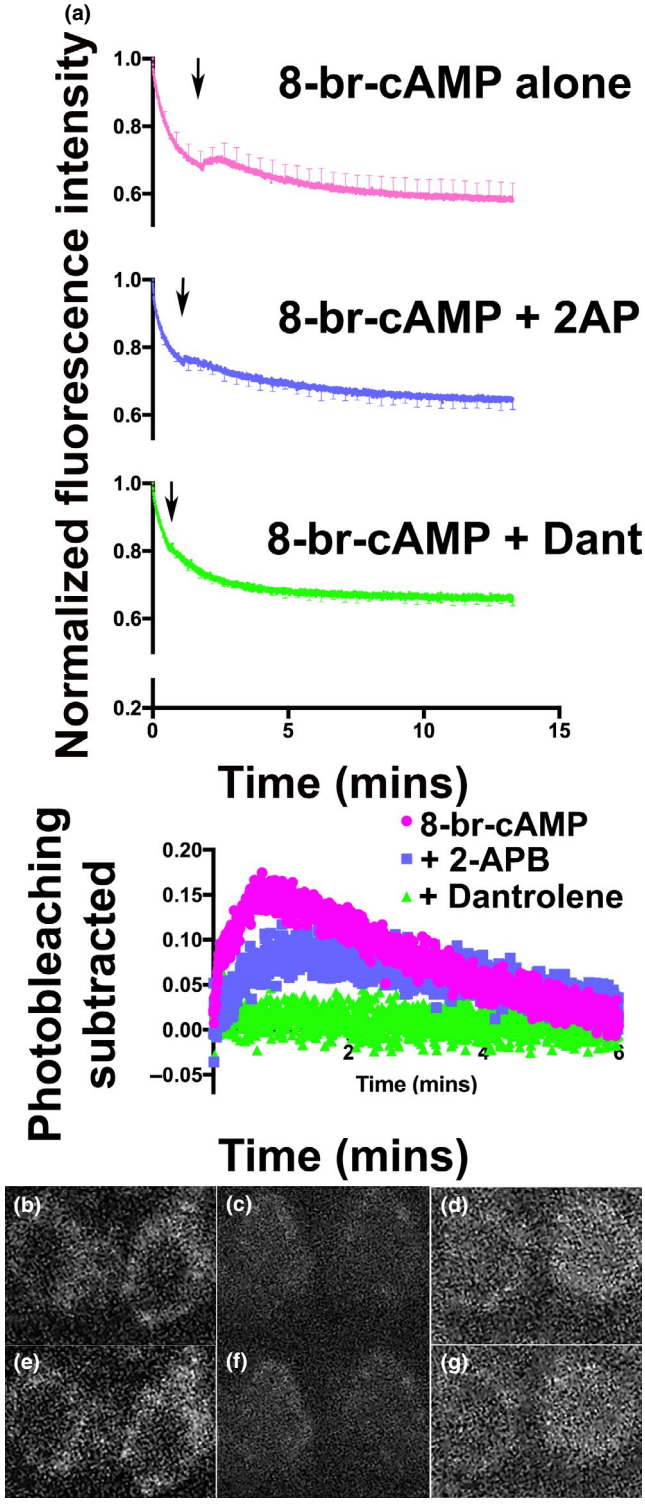

FIGURE 8 Addition of 8-br-cAMP increases Ca^{2+} signal in hair cells that is attenuated in the presence of inhibitors of CICR. (a) Shown are Ca^{2+} fluorescence signal (detected after incubating cells in 1 μM Fluo-3-AM in perilymph containing 1.3 mM Ca^{2+} for 30 min) in hair cells as a function of time. The addition of 100 μM 8-br-cAMP (arrow) resulted in an increase in Ca^{2+} in the cell above the exponential decay in fluorescence due to photobleaching. In contrast, the presence of 2-APB and dantrolene (both inhibitors of CICR) attenuated (2-APB) and eliminated (dantrolene) the increase in Ca^{2+} signal induced by 100 μM 8-br-cAMP. In order to make comparable measurements, Ca^{2+} signal in the entire cell was measured, since inhibitors of CICR caused a significant reduction in peripheral Ca^{2+} signal. The lowest panel shows the increase in Ca^{2+} signal from which the exponential decay from photobleaching was subtracted. In this panel, the fluorescence signal was synchronized to the point at which 8-br-cAMP was added. Error bars are *SEM*. (b,c,d,e,f,g) Ca^{2+} imaging of individual hair cells before (b - 8-br-cAMP alone, d – 8-br-cAMP plus 2-APB, f – 8-br-cAMP plus Dantrolene) and after (c - 8-br-cAMP alone, e – 8-br-cAMP plus 2-APB, g - 8-br-cAMP plus Dantrolene) treatment with 8-Br cAMP. Cells were preloaded with 1 μM Fluor3 and the respective inhibitors for 30 min at RT C in perilymph containing 1.3 mM Ca^{2+}

discovered the effects of CICR while exploring the effects of protein kinase A on BK channel kinetics in chick hair cells. We present three streams of data that substantiate our findings. Electrophysiological data showing a reduced current that was accompanied by a significant depolarizing shift in the normalized G–V relationship with BAPTA compared to EGTA in nominally 0 μM Ca^{2+} suggested that higher spatial buffering afforded by BAPTA significantly limited Ca^{2+} available to activate BK channels. EGTA has a slower rate of Ca^{2+} binding (compared to BAPTA) and allows for more spatially diffuse Ca^{2+} signaling (Augustine, Adler, & Charlton, 1991; Neher, 1998; Rios & Stern, 1997). Preventing Ca^{2+} entry by blocking VGCCs and reducing extracellular Ca^{2+} both resulted in a depolarizing shift in the normalized G–V relationship. These data suggested that entry of extracellular Ca^{2+} is important for activation of BK channels likely by raising Ca^{2+} concentrations in the vicinity of BK channels clustered and co-localized with VGCCs at the plasma membrane of hair cells. Furthermore, when using EGTA as the intracellular buffer we note an increase in the size of current with no significant change in the normalized G–V relationship when intracellular Ca^{2+} was raised from 0 to 10 and then to 100 μM Ca^{2+}. Since the use of BAPTA shifted the normalized G–V relationship in a depolarizing direction compared to EGTA with comparable Ca^{2+} concentrations (0 μM), these data suggest that (1) local concentrations of Ca^{2+} in the presence of EGTA were saturating and (2) recruiting more BK channels are effected by higher Ca^{2+} concentrations. These data imply that BK channels are activated by two mechanisms—by entry of Ca^{2+} through VGCCs, and, farther from VGCCs, through CICR. In fact, previous confocal data have shown that majority VGCC to be in proximity to BK channels, but the majority of BK channels were spatially separated from VGCCs (Samaranayake et al., 2004). Currents in the presence of BAPTA were 20%–25% of that in the presence of EGTA (both with nominally 0 μM Ca^{2+}). These data argue that BK channels in approximation with VGCCs are only a fraction of BK channels in hair cells confirming prior confocal data.

When cells were perfused with forskolin we see a similar effect to that of raising pipette Ca^{2+} concentrations, namely, an increase in the size of the current. Since PKA is a

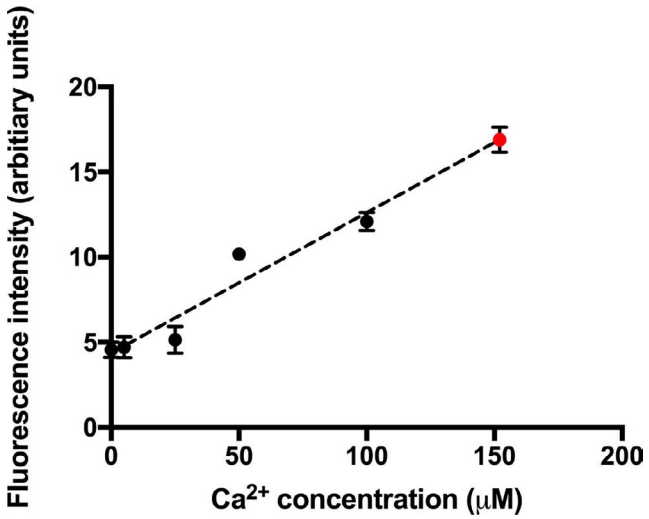

FIGURE 9 Ca^{2+} concentrations at the periphery of hair cells exceed a 100 μM. Shown is the average fluorescence intensity of hair cells with different bath concentrations of Ca^{2+}. Basilar papillae from chicks were incubated in the presence of the Ca^{2+} ionophore A23187 and different concentrations of Ca^{2+} (nominally 0 μM Ca^{2+}, 5 μM Ca^{2+}, 25 μM Ca^{2+}, 50 μM Ca^{2+}, and 100 μM Ca^{2+}). Fluorescence (in arbitrary units) was measured away from clusters to prevent CICR skewing our data. Measurements from 8 to 12 cells were averaged. Also shown (in red) is the average fluorescence intensity of Ca^{2+} clusters along the periphery of the cell in hair cells incubated in the presence of perilymph containing 1.3 mM Ca^{2+}. The concentration of Ca^{2+} is in excess of 100 μM based on its fluorescence measures. Using a linear trend line, we estimate a value of 150 μM Ca^{2+}. In all these measures, we averaged the fluorescence from clusters at the periphery of 8–10 hair cells

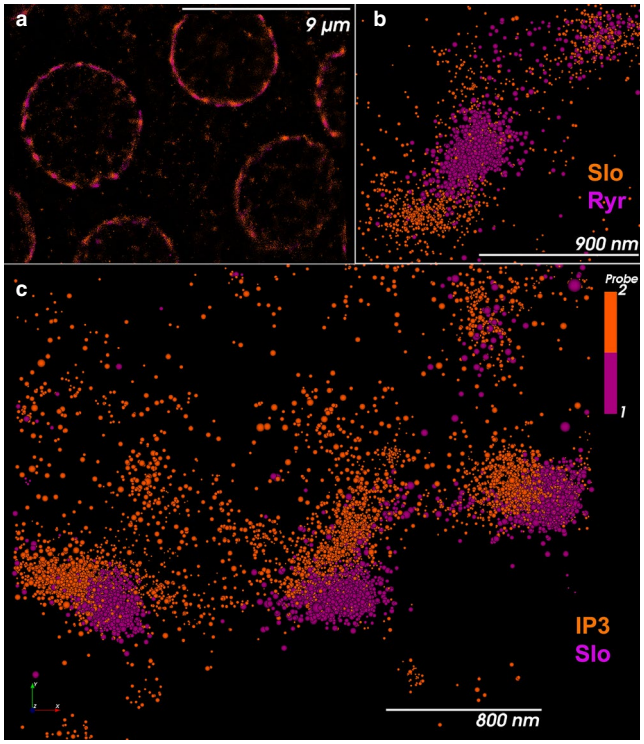

FIGURE 10 Slo channels lie in close proximity to IP3 receptors and ryanodine receptors. STORM images of individual hair cells in the basilar papilla are visualized end on from above. **a,b.** Slo channel puncta (purple) are localized in close proximity to IP3 receptors (orange) in low (a) and higher magnifications (b). Slo channel puncta lie close to the membrane with IP3 receptors arranged tangentially away from the membrane. In many instances, we could not separate the two clusters in two dimensions. Where such separation was possible, the distance between the clusters was usually less than 100 nm (see below). (c) Slo channels (orange) are also seen in proximity to ryanodine receptors (purple). Here too, the two protein clusters were often not separable in two dimensions. Where the clusters were separable, the distance between them was usually less than 150 nm (see below)

well-known activator of CICR and since the effects of PKA activation were dependent on pipette Ca^{2} concentration, we reason that CICR is the principle mechanism by which PKA (and raising pipette Ca^{2+} concentrations) affects BK channels. A decrease in the size of the current with specific inhibitors to both IP3 and ryanodine receptors and its prevention of forskolin-induced increases in BK currents confirmed the occurrence of CICR with PKA activation.

We note differential effects of blockers of ryanodine and IP3 receptors in the presence of PKA activation. In contrast to dantrolene and forskolin, we note a greater reduction in the size of the current and a depolarizing shift in the normalized G–V relationship when forskolin and 2APB were used in combination. One possible explanation for this result is a greater functional coupling between BK channels and IP3 receptors.

Imaging with the Ca^{2+} indicator dye Fluo-3-AM demonstrated high concentrations of Ca^{2+} along the periphery of hair cells that were clustered. The signal within these peripheral clusters was attenuated by reducing external Ca^{2+} concentration, and, separately, in the presence of inhibitors of CICR with high external Ca^{2+}. Moreover, measures of Ca^{2+} concentration at the periphery of the cell using fluorescence were concordant with our electrophysiological data and supersaturating. We use the term supersaturating to mean that a change in Ca^{2+} did not result in a change in voltage sensitivity (Art et al., 1995; Bai et al., 2011; Duncan & Fuchs, 2003; Roberts, 1993; Tucker & Fettiplace, 1995). We confirm a rise in intracellular Ca^{2+} concentrations in response to PKA activation and an attenuation or absent rise in this signal in response to PKA activation by inhibition of CICR. Together, the Ca^{2+} imaging data confirm and reinforce our electrophysiological data. Finally, using super-resolution microscopy, we confirm the presence of both IP3 and ryanodine receptors to lie within 100 nm of BK channels along the periphery of the cell.

4.1 | Nanodomains versus microdomains

In sum, our data argue for a close approximation of BK channels and CICR. Over what distances does Ca^{2+} act? This is a

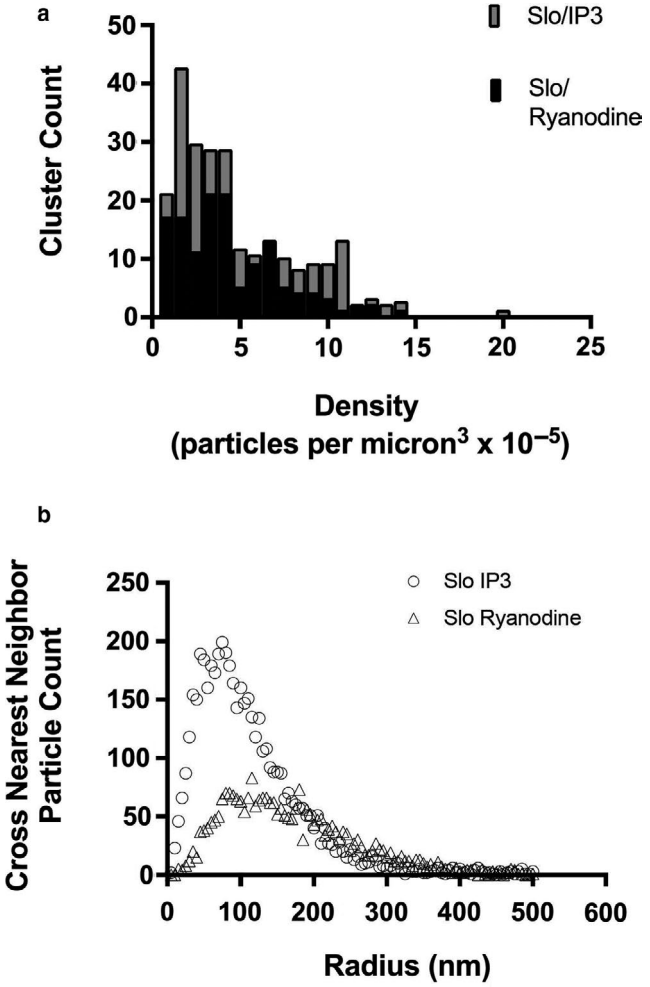

FIGURE 11 Slo, IP3 receptors, and ryanodine receptors are clustered and lie within nano–micro domains. (a) Slo, IP3 and ryanodine receptors were clustered. Shown is the distribution in the density of particles and its variability with cluster number. The histogram of binned data shows a skewed distribution in particles. Both Slo/IP3 and Slo/ryanodine clusters show similar patterns of clustering. There was over a tenfold range in particle density in clusters. (b) Using a nearest neighbor algorithm, we find a skewed distribution in the distances between Slo and IP3 receptors, and, separately, Slo and ryanodine receptors. Shown are histograms of crossed (that is centroids of Slo and IP3 particles, and, separately, centroids of Slo and ryanodine particles) nearest neighbor distances. The distances between Slo and IP3 receptors started at 5 nm, and the distances between Slo and ryanodine receptors started at 15 nm. The peak in the distribution of distances between Slo and IP3 lay between 55 and 85 nm. The peak in distribution of distances between Slo and ryanodine receptors lay between 100 and 135 nm. Using a 200-nm cutoff radius, the median nearest neighbor distance was 85 nm for Slo/IP3 particles, and 100 nm for Slo/ ryanodine receptor particles

key question as it will determine how electrical resonance is affected by CICR in hair cells. Nanodomains have been referred to over distances of 20 nm, while microdomains refer to distances of 200 nm (Neher, 1998). Using this definition, prior work in the frog saccule suggested microdomains of Ca^{2+} with synaptic release sites within 300 nm from Ca^{2+} channels (Roberts et al., 1990). While the high concentrations of local Ca^{2+} we observe and the differential responses to BAPTA and EGTA are consistent with nanodomains of Ca^{2+}(Augustine et al., 2003; Heidelberger et al., 1994), our measured distances between BK channels and IP3 and ryanodine receptors extend from distances consistent with nanodomains to intermediate distances between nanodomains and microdomains. The distance between Slo and IP3 receptors and Slo and ryanodine receptors start at 5 nm and 15 nm, respectively. The peak in distribution of distances between BK channels and IP3 receptors was 55–85 nm. In contrast, the peak in the distribution of distances between BK channels and ryanodine receptors lay between 100 and 135 nm.

4.2 | How does PKA affect CICR?

How might PKA activation influence CICR in hair cells? CICR has been a most well-studied phenomenon in muscle cells, endocrine cells, and neuronal cells (Roderick, Berridge, & Bootman, 2003). ITPRs acting as coincident detectors (requiring both IP3 and Ca^{2+} for activation) and ryanodine receptors that respond to Ca^{2+} have been well-studied in this context (Roderick et al., 2003). PKA increases CICR by affecting a multitude of processes in this cascade. Thus, PKA phosphorylates both ITP3Rs (ITP3R1 and ITP3R3) and ryanodine receptors 1 and 2 to increase their sensitivity to intracellular Ca^{2+}, thus, increasing CICR (Dyachok & Gylfe, 2004; Holz, Leech, Heller, Castonguay, & Habener, 1999; Islam et al., 1998; Reiken et al., 2003; Taylor, 2017; Wehrens et al., 2006). Interrogation of prior published chicken Affymetrix datasets reveals that ITPR1, 2, and 3 are all detected in the basilar papilla (Frucht et al., 2011). Similarly, RYR1, 2, and 3 are all detected in the basilar papilla with no significant differential distribution of these receptors along the tonotopic axis (Itpr1, Itpr2, and Ryr1 are also expressed in mouse inner and outer hair cells) (Frucht et al., 2011; Li et al., 2018). In addition to the effects on ITPRs and ryanodine receptors, PKA also modulates phospholipase C (PLC) and couples it to receptors strengthening CICR (Liu & Simon, 1996). Finally, PKA has been shown to phosphorylate Cav1.3 increasing its conductance (Mahapatra, Marcantoni, Zuccotti, Carabelli, & Carbone, 2012). Our data showing a block of PKA effects by inhibiting CICR suggests that the effects of PKA are predominantly effected through CICR and not through effects on Cav 1.3.

4.3 | Effects on electrical resonance

What effects might CICR have on electrical resonance? While we did not explore the effects of PKA activation and

CICR on electrical resonance, our initial impetus to studying PKA effects on BK currents was to explore how varying BK channel kinetics occur in hair cells along the tonotopic axis. Varying BK channel kinetics is the principal mechanism for frequency tuning and electrical resonance in the turtle (Art et al., 1995). There are data showing a similar mechanism operates in the chick (Fettiplace & Fuchs, 1999; Fuchs et al., 1988).

The close proximity of IP3 and ryanodine receptors to BK channels could extend the distance of Ca^{2+} signaling, thereby extending its operational range. This could explain the larger currents observed with CICR from an increasing number of BK channels activated farther from the site of Ca^{2+} entry. On the other hand, CICR could simultaneously potentially attenuate the temporal fidelity of electrical resonance from the increased duration of feedback inhibition. Other variables that affect the sharpness of the negative feedback loop between voltage-gated Ca^{2+} channels and BK channels are the distance between these two channels (estimated to be 50nm), the number of Ca^{2+} and BK channels at these local clusters, and the effective buffering of the many different native Ca^{2+} buffers (Roberts, 1993, 1994; Wu, Art, Goodman, & Fettiplace, 1995). Previous modeling experiments in the turtle have incorporated these variables and produced a reasonable approximation to experimental data (Wu, Tucker, & Fettiplace, 1996). Our data showing CICR and its effects on BK channels would necessitate a rethinking of these models, particularly if CICR is shown to operate in the turtle, as well. With data showing complex control and kinetics of CICR in other systems, our data in turn point to increasingly complex control of electrical resonance (Dyachok & Gylfe, 2004).

Our data with whole-cell recordings showed no change in the voltage dependence of BK currents with 100 μM, 10 μM and nominally 0 μM intracellular Ca^{2+} when EGTA was used as a buffer. On face value, these data could be taken to imply that the concentration of Ca^{2+} in proximity to BK channels are a 100 μM even when the pipette Ca^{2+} concentration was nominally 0 μM Ca^{2+} owing to the limited spatial buffering of EGTA with (extracellular) Ca^{2+} entry occurring through voltage-gated channels. Our measurements of Ca^{2+} concentration as exceeding 100 μM, albeit in the native state where buffering capacity is not precisely defined (hair cells contain mM concentrations of Ca^{2+} buffer), are consistent with this possibility.

The high local concentration of Ca^{2+} is also consistent with electrophysiological measurements of Ca^{2+} sensitivity of BK channels in these hair cells. Duncan et al., using excised patch recordings, demonstrated a half-maximal Ca^{2+} sensitivity of 0.1–5 μM Ca^{2+} at +50mV (the voltage at which our measurements of currents in whole-cell recordings were robust) (Duncan & Fuchs, 2003). Close to the resting membrane potential of hair cells (−50mV), these authors determine a half-maximal Ca^{2+} concentration of 5–100 μM (although at the frequency location we used—20%–30% from the apical end—the concentration was closer to 5–50 μM).

The high local concentration of Ca^{2+} in proximity to BK channels from CICR could also explain the seeming discrepancy in in vivo findings of minimal differences in Ca^{2+} sensitivity compared to the large differences in Ca^{2+} sensitivity observed when splice variants were expressed in heterologous systems (Art et al., 1995; Duncan & Fuchs, 2003; Jones et al., 1999; Ramanathan et al., 1999, 2000). Excised patches used to determine sensitivity to Ca^{2+} would presumably also contain IP3 and ryanodine receptors that in turn would induce the local release of Ca^{2+}.

4.4 | Other implications of cicr in hair cells

Synaptic vesicle release is the other mechanism that is affected by Ca^{2+} entry into the base of hair cells. How might CICR affect synaptic release in hair cells? Increasing BK current size with no effects of its voltage sensitivity points to a spatially enlarging Ca^{2+} signal with CICR in chick hair cells. A spatially extended Ca^{2+} signal could also increase the release of synaptic vesicles. In fact, such a possibility has been suggested by experimental data in turtles (with corroborating data from mice and rats). Real-time measurements of synaptic release (capacitance measures) and Ca^{2+} imaging show a linear and supralinear relationship between cell Ca^{2+} and synaptic release in inner hair cells (Schnee, Santos-Sacchi, Castellano-Munoz, Kong, & Ricci, 2011). The supralinear release was correlated with an additional intracellular source of Ca^{2+} and was speculated to be responsible for recruiting the reserve pool of vesicles.

Our findings may have evolutionary parallels in mammalian inner hair cells. In mammalian inner hair cells, Marcotti et al. (2003) demonstrated the presence of CICR through Ryanodine receptors. In these cells, the majority of BK channels lie at the "neck" of these cells and are positionally independent of VGCC (a small fraction of BK channels are present at the base of the cells in proximity to VGCCs as in chick hair cells) (Marcotti et al., 2003). The mechanism of activation of BK channels at the neck of these cells is likely through both CICR and an enhanced voltage/ Ca2+ sensitivity brought about by association with auxillary subunits as suggested by more recent data (Lingle et al., 2019; Marcotti et al., 2003; Oliver, Knipper, Derst, & Fakler, 2003; Xue, Lawal, Bai, Santos-Sacchi, & Navaratnam, 2020).

In conclusion, we show that CICR resides in hair cells in close proximity to BK channels. We provide electrophysiological, confocal Ca^{2+} imaging, and super-resolution fluorescence immunolocalization data to support our conclusion that CICR likely plays an important role in hair cell function. These data require a rethinking of the physiological and

molecular mechanisms of electrical resonance and synaptic vesicle release.

ACKNOWLEDGMENTS

We acknowledge Drs Barbara Ehrlich and Len Kaczmarek for critical reading of the manuscript.

CONFLICTS OF INTEREST

There were no conflicts of interest.

AUTHOR CONTRIBUTIONS

JPB, NX, and DSN designed and performed experiments, and prepared the manuscript. OL and AN designed and performed experiments. JSS designed experiments and prepared the manuscript.

ORCID

Dhasakumar Navaratnam https://orcid.org/0000-0002-5431-8191

REFERENCES

Art, J. J., Wu, Y. C., & Fettiplace, R. (1995). The calcium-activated potassium channels of turtle hair cells. *The Journal of General Physiology*, *105*, 49–72. https://doi.org/10.1085/jgp.105.1.49

Augustine, G. J., Adler, E. M., & Charlton, M. P. (1991). The calcium signal for transmitter secretion from presynaptic nerve terminals. *Annals of the New York Academy of Sciences*, *635*, 365–381. https://doi.org/10.1111/j.1749-6632.1991.tb36505.x

Augustine, G. J., Santamaria, F., & Tanaka, K. (2003). Local calcium signaling in neurons. *Neuron*, *40*, 331–346. https://doi.org/10.1016/S0896-6273(03)00639-1

Bai, J. P., Surguchev, A., Joshi, P., Gross, L., & Navaratnam, D. (2012b). CDK5 interacts with Slo and affects its surface expression and kinetics through direct phosphorylation. *American Journal of Physiology. Cell Physiology*, *302*, C766–780. https://doi.org/10.1152/ajpcell.00339.2011

Bai, J. P., Surguchev, A., & Navaratnam, D. (2011). beta4-subunit increases Slo responsiveness to physiological Ca2+ concentrations and together with beta1 reduces surface expression of Slo in hair cells. *American Journal of Physiology Cell Physiology*, *300*, C435–446.

Brenner, R., Chen, Q. H., Vilaythong, A., Toney, G. M., Noebels, J. L., & Aldrich, R. W. (2005). BK channel beta4 subunit reduces dentate gyrus excitability and protects against temporal lobe seizures. *Nature Neuroscience*, *8*, 1752–1759.

Brenner, R., Jegla, T. J., Wickenden, A., Liu, Y., & Aldrich, R. W. (2000). Cloning and functional characterization of novel large conductance calcium-activated potassium channel beta subunits, hKCNMB3 and hKCNMB4. *Journal of Biological Chemistry*, *275*, 6453–6461.

Chen, L., Tian, L., MacDonald, S. H., McClafferty, H., Hammond, M. S., Huibant, J. M., … Shipston, M. J. (2005). Functionally diverse complement of large conductance calcium- and voltage-activated potassium channel (BK) alpha-subunits generated from a single site of splicing. *Journal of Biological Chemistry*, *280*, 33599–33609.

Crawford, A. C., & Fettiplace, R. (1981). An electrical tuning mechanism in turtle cochlear hair cells. *Journal of Physiology*, *312*, 377–412. https://doi.org/10.1113/jphysiol.1981.sp013634

Dedkova, E. N., Sigova, A. A., & Zinchenko, V. P. (2000). Mechanism of action of calcium ionophores on intact cells: Ionophore-resistant cells. *Membr Cell Biol*, *13*, 357–368.

Duncan, R. K., & Fuchs, P. A. (2003). Variation in large-conductance, calcium-activated potassium channels from hair cells along the chicken basilar papilla. *Journal of Physiology*, *547*, 357–371. https://doi.org/10.1113/jphysiol.2002.029785

Dyachok, O., & Gylfe, E. (2004). Ca(2+)-induced Ca(2+) release via inositol 1,4,5-trisphosphate receptors is amplified by protein kinase A and triggers exocytosis in pancreatic beta-cells. *Journal of Biological Chemistry*, *279*, 45455–45461.

Fettiplace, R., & Fuchs, P. A. (1999). Mechanisms of hair cell tuning. *Annual Review of Physiology*, *61*, 809–834. https://doi.org/10.1146/annurev.physiol.61.1.809

Frucht, C. S., Uduman, M., Kleinstein, S. H., Santos-Sacchi, J., & Navaratnam, D. S. (2011). Gene expression gradients along the tonotopic axis of the chicken auditory epithelium. *Journal of the Association for Research in Otolaryngology : JARO*, *12*, 423–435. https://doi.org/10.1007/s10162-011-0259-2

Fuchs, P. A., & Evans, M. G. (1990). Potassium currents in hair cells isolated from the cochlea of the chick. *Journal of Physiology*, *429*, 529–551. https://doi.org/10.1113/jphysiol.1990.sp018271

Fuchs, P. A., & Lauer, A. M. (2019). Efferent Inhibition of the Cochlea. *Cold Spring Harbor Perspectives in Medicine*, *9*. https://doi.org/10.1101/cshperspect.a033530

Fuchs, P. A., Nagai, T., & Evans, M. G. (1988). Electrical tuning in hair cells isolated from the chick cochlea. *Journal of Neuroscience*, *8*, 2460–2467. https://doi.org/10.1523/JNEUROSCI.08-07-02460.1988

Fuchs, P. A., & Sokolowski, B. H. (1990). The acquisition during development of Ca-activated potassium currents by cochlear hair cells of the chick. *Proceedings of the Royal Society of London. Series B: Biological Sciences*, *241*, 122–126.

Gan, G., Yi, H., Chen, M., Sun, L., Li, W., Wu, Y., & Ding, J. (2008). Structural basis for toxin resistance of beta4-associated calcium-activated potassium (BK) channels. *Journal of Biological Chemistry*, *283*, 24177–24184.

Heidelberger, R., Heinemann, C., Neher, E., & Matthews, G. (1994). Calcium dependence of the rate of exocytosis in a synaptic terminal. *Nature*, *371*, 513–515. https://doi.org/10.1038/371513a0

Hodgkin, A. L., & Huxley, A. F. (1952). A quantitative description of membrane current and its application to conduction and excitation in nerve. *Journal of Physiology*, *117*, 500–544. https://doi.org/10.1113/jphysiol.1952.sp004764

Holz, G. G., Leech, C. A., Heller, R. S., Castonguay, M., & Habener, J. F. (1999). cAMP-dependent mobilization of intracellular Ca2+ stores by activation of ryanodine receptors in pancreatic beta-cells. A Ca2+ signaling system stimulated by the insulinotropic hormone glucagon-like peptide-1-(7–37). *Journal of Biological Chemistry*, *274*, 14147–14156.

Irie, T., & Trussell, L. O. (2017). Double-nanodomain coupling of calcium channels, ryanodine receptors, and BK channels controls the generation of burst firing. *Neuron*, *96*(856–870), e854. https://doi.org/10.1016/j.neuron.2017.10.014

Islam, M. S., Leibiger, I., Leibiger, B., Rossi, D., Sorrentino, V., Ekstrom, T. J., … Berggren, P. O. (1998). In situ activation of the type 2 ryanodine receptor in pancreatic beta cells requires cAMP-dependent phosphorylation. *Proceedings of the National Academy of Sciences of the United States of America*, *95*, 6145–6150. https://doi.org/10.1073/pnas.95.11.6145

Issa, N. P., & Hudspeth, A. J. (1994). Clustering of Ca2+ channels and Ca(2+)-activated K+ channels at fluorescently labeled presynaptic active zones of hair cells. *Proceedings of the National Academy of Sciences of the United States of America*, *91*, 7578–7582. https://doi.org/10.1073/pnas.91.16.7578

Jones, E. M., Gray-Keller, M., Art, J. J., & Fettiplace, R. (1999). The functional role of alternative splicing of Ca(2+)-activated K+ channels in auditory hair cells. *Annals of the New York Academy of Sciences*, *868*, 379–385. https://doi.org/10.1111/j.1749-6632.1999.tb11299.x

Jones, S. M., & Jones, T. A. (1995). The tnotopic map of the embryonic chick cochlea. *Hearing Research*, *82*, 149–157.

Li, Y., Liu, H., Giffen, K. P., Chen, L., Beisel, K. W., & He, D. Z. Z. (2018). Transcriptomes of cochlear inner and outer hair cells from adult mice. *Scientific Data*, *5*, 180199. https://doi.org/10.1038/sdata.2018.199

Lingle, C. J., Martinez-Espinosa, P. L., Yang-Hood, A., Boero, L. E., Payne, S., Persic, D., … Rutherford, M. A. (2019). LRRC52 regulates BK channel function and localization in mouse cochlear inner hair cells. *Proceedings of the National Academy of Sciences of the United States of America*, *116*, 18397–18403. https://doi.org/10.1073/pnas.1907065116

Liu, M., & Simon, M. I. (1996). Regulation by cAMP-dependent protein kinase of a G-protein-mediated phospholipase C. *Nature*, *382*, 83–87. https://doi.org/10.1038/382083a0

Mahapatra, S., Marcantoni, A., Zuccotti, A., Carabelli, V., & Carbone, E. (2012). Equal sensitivity of Cav1.2 and Cav1.3 channels to the opposing modulations of PKA and PKG in mouse chromaffin cells. *Journal of Physiology*, *590*, 5053–5073. https://doi.org/10.1113/jphysiol.2012.236729

Marcotti, W., Johnson, S. L., Holley, M. C., & Kros, C. J. (2003). Developmental changes in the expression of potassium currents of embryonic, neonatal and mature mouse inner hair cells. *Journal of Physiology*, *548*, 383–400. https://doi.org/10.1113/jphysiol.2002.034801

Marcotti, W., Johnson, S. L., & Kros, C. J. (2004). Effects of intracellular stores and extracellular Ca(2+) on Ca(2+)-activated K(+) currents in mature mouse inner hair cells. *Journal of Physiology*, *557*, 613–633.

Meera, P., Wallner, M., & Toro, L. (2000). A neuronal beta subunit (KCNMB4) makes the large conductance, voltage- and Ca2+-activated K+ channel resistant to charybdotoxin and iberiotoxin. *Proceedings of the National Academy of Sciences of the United States of America*, *97*, 5562–5567. https://doi.org/10.1073/pnas.100118597

Miranda-Rottmann, S., Kozlov, A. S., & Hudspeth, A. J. (2010). Highly specific alternative splicing of transcripts encoding BK channels in the chicken's cochlea is a minor determinant of the tonotopic gradient. *Molecular and Cellular Biology*, *30*, 3646–3660. https://doi.org/10.1128/MCB.00073-10

Neher, E. (1998). Vesicle pools and Ca2+ microdomains: New tools for understanding their roles in neurotransmitter release. *Neuron*, *20*, 389–399. https://doi.org/10.1016/S0896-6273(00)80983-6

Oliver, D., Knipper, M., Derst, C., & Fakler, B. (2003). Resting potential and submembrane calcium concentration of inner hair cells in the isolated mouse cochlea are set by KCNQ-type potassium channels. *Journal of Neuroscience*, *23*, 2141–2149. https://doi.org/10.1523/JNEUROSCI.23-06-02141.2003

Purcell, E. K., Liu, L., Thomas, P. V., & Duncan, R. K. (2011). Cholesterol influences voltage-gated calcium channels and BK-type potassium channels in auditory hair cells. *PLoS ONE*, *6*, e26289. https://doi.org/10.1371/journal.pone.0026289

Ramanathan, K., Michael, T. H., & Fuchs, P. A. (2000). beta subunits modulate alternatively spliced, large conductance, calcium-activated potassium channels of avian hair cells. *Journal of Neuroscience*, *20*, 1675–1684.

Ramanathan, K., Michael, T. H., Jiang, G. J., Hiel, H., & Fuchs, P. A. (1999). A molecular mechanism for electrical tuning of cochlear hair cells. *Science*, *283*, 215–217. https://doi.org/10.1126/science.283.5399.215

Reiken, S., Lacampagne, A., Zhou, H., Kherani, A., Lehnart, S. E., Ward, C., … Marks, A. R. (2003). PKA phosphorylation activates the calcium release channel (ryanodine receptor) in skeletal muscle: Defective regulation in heart failure. *Journal of Cell Biology*, *160*, 919–928. https://doi.org/10.1083/jcb.200211012

Reinhart, P. H., Chung, S., & Levitan, I. B. (1989). A family of calcium-dependent potassium channels from rat brain. *Neuron*, *2*, 1031–1041. https://doi.org/10.1016/0896-6273(89)90227-4

Ricci, A. J., Bai, J. P., Song, L., Lv, C., Zenisek, D., & Santos-Sacchi, J. (2013). Patch-clamp recordings from lateral line neuromast hair cells of the living zebrafish. *Journal of Neuroscience*, *33*, 3131–3134. https://doi.org/10.1523/JNEUROSCI.4265-12.2013

Rios, E., & Stern, M. D. (1997). Calcium in close quarters: Microdomain feedback in excitation-contraction coupling and other cell biological phenomena. *Annual Review of Biophysics and Biomolecular Structure*, *26*, 47–82. https://doi.org/10.1146/annurev.biophys.26.1.47

Roberts, W. M. (1993). Spatial calcium buffering in saccular hair cells. *Nature*, *363*, 74–76. https://doi.org/10.1038/363074a0

Roberts, W. M. (1994). Localization of calcium signals by a mobile calcium buffer in frog saccular hair cells. *Journal of Neuroscience*, *14*, 3246–3262. https://doi.org/10.1523/JNEUROSCI.14-05-03246.1994

Roberts, W. M., Jacobs, R. A., & Hudspeth, A. J. (1990). Colocalization of ion channels involved in frequency selectivity and synaptic transmission at presynaptic active zones of hair cells. *Journal of Neuroscience*, *10*, 3664–3684. https://doi.org/10.1523/JNEUROSCI.10-11-03664.1990

Roderick, H. L., Berridge, M. J., & Bootman, M. D. (2003). Calcium-induced calcium release. *Current Biology*, *13*, R425. https://doi.org/10.1016/S0960-9822(03)00358-0

Rohmann, K. N., Wersinger, E., Braude, J. P., Pyott, S. J., & Fuchs, P. A. (2015). Activation of BK and SK channels by efferent synapses on outer hair cells in high-frequency regions of the rodent cochlea. *Journal of Neuroscience*, *35*, 1821–1830. https://doi.org/10.1523/JNEUROSCI.2790-14.2015

Sabourin, J., Boet, A., Rucker-Martin, C., Lambert, M., Gomez, A. M., Benitah, J. P., … Antigny, F. (2018). Ca(2+) handling remodeling and STIM1L/Orai1/TRPC1/TRPC4 upregulation in monocrotaline-induced right ventricular hypertrophy. *Journal of Molecular and Cellular Cardiology*, *118*, 208–224. https://doi.org/10.1016/j.yjmcc.2018.04.003

Samaranayake, H., Saunders, J. C., Greene, M. I., & Navaratnam, D. S. (2004). Ca(2+) and K(+) (BK) channels in chick hair cells are clustered and colocalized with apical-basal and tonotopic gradients. *Journal of Physiology*, *560*, 13–20.

Saunders, J. C., Coles, R. B., & Gates, G. R. (1973). The development of auditory evoked responses in the cochlea and cochlear nuclei of the chick. *Brain Research*, *63*, 59–74. https://doi.org/10.1016/0006-8993(73)90076-0

Schnee, M. E., Santos-Sacchi, J., Castellano-Munoz, M., Kong, J. H., & Ricci, A. J. (2011). Calcium-dependent synaptic vesicle trafficking underlies indefatigable release at the hair cell afferent fiber synapse. *Neuron*, *70*, 326–338. https://doi.org/10.1016/j.neuron.2011.01.031

Surguchev, A., Bai, J. P., Joshi, P., & Navaratnam, D. (2012). Hair cell BK channels interact with RACK1, and PKC increases its expression on the cell surface by indirect phosphorylation. *American Journal of Physiology-Cell Physiology*, *303*, C143–150. https://doi.org/10.1152/ajpcell.00062.2012

Tadevosyan, A., Xiao, J., Surinkaew, S., Naud, P., Merlen, C., Harada, M., … Nattel, S. (2017). Intracellular Angiotensin-II interacts with nuclear angiotensin receptors in cardiac fibroblasts and regulates RNA synthesis, cell proliferation, and collagen secretion. *Journal of the American Heart Association*, *6*. https://doi.org/10.1161/JAHA.116.004965

Taylor, C. W. (2017). Regulation of IP3 receptors by cyclic AMP. *Cell Calcium*, *63*, 48–52. https://doi.org/10.1016/j.ceca.2016.10.005

Tian, L., Duncan, R. R., Hammond, M. S., Coghill, L. S., Wen, H., Rusinova, R., … Shipston, M. J. (2001). Alternative splicing switches potassium channel sensitivity to protein phosphorylation. *Journal of Biological Chemistry*, *276*, 7717–7720. https://doi.org/10.1074/jbc.C000741200

Tilney, L. G., Tilney, M. S., Saunders, J. S., & DeRosier, D. J. (1986). Actin Filaments, stereocillia, and hair cells of the bird cochlea III. The development of differentiation of hair cells and stereocillia. *Developmental Biology*, *116*, 100–118.

Tucker, T., & Fettiplace, R. (1995). Confocal imaging of calcium microdomains and calcium extrusion in turtle hair cells. *Neuron*, *15*, 1323–1335. https://doi.org/10.1016/0896-6273(95)90011-X

Wehrens, X. H., Lehnart, S. E., Reiken, S., Vest, J. A., Wronska, A., & Marks, A. R. (2006). Ryanodine receptor/calcium release channel PKA phosphorylation: A critical mediator of heart failure progression. *Proceedings of the National Academy of Sciences of the United States of America*, *103*, 511–518. https://doi.org/10.1073/pnas.0510113103

Wu, Y. C., Art, J. J., Goodman, M. B., & Fettiplace, R. (1995). A kinetic description of the calcium-activated potassium channel and its application to electrical tuning of hair cells. *Progress in Biophysics and Molecular Biology*, *63*, 131–158. https://doi.org/10.1016/0079-6107(95)00002-5

Wu, Y. C., Tucker, T., & Fettiplace, R. (1996). A theoretical study of calcium microdomains in turtle hair cells. *Biophysical Journal*, *71*, 2256–2275. https://doi.org/10.1016/S0006-3495(96)79429-8

Xue, N., Lawal, L., Bai, J., Santos-Sacchi, J., & Navaratnam, D. (2020). STORM imaging reveals Calcium nanodomains in proximity to BK channels in hair cells of the mouse and chick. 43rd Annual Midwinter Meeting of the Association in Research in Otolaryngology PS915. Retrieved from https://aro.org/wp-content/uploads/2020/02/2020-Abstracts_1-21-20-Web.pdf

Zhong, S., Navaratnam, D., & Santos-Sacchi, J. (2014). A genetically-encoded YFP sensor with enhanced chloride sensitivity, photostability and reduced ph interference demonstrates augmented transmembrane chloride movement by gerbil prestin (SLC26a5). *PLoS ONE*, *9*, e99095. https://doi.org/10.1371/journal.pone.0099095

Zhong, S., Rivera-Molina, F., Rivetta, A., Toomre, D., Santos-Sacchi, J., & Navaratnam, D. (2019). Seeing the long tail: A novel green fluorescent protein, SiriusGFP, for ultra long timelapse imaging. *Journal of Neuroscience Methods*, *313*, 68–76. https://doi.org/10.1016/j.jneumeth.2018.12.008

How to cite this article: Bai J-P, Xue N, Lawal O, Nyati A, Santos-Sacchi J, Navaratnam D. Calcium-induced calcium release in proximity to hair cell BK channels revealed by PKA activation. *Physiol Rep*. 2020;8:e14449. https://doi.org/10.14814/phy2.14449